Int. J. Heat Mass Transfer. Vol. 33, No. 5, pp. 859–867, 1990
Printed in Great Britain

0017–9310/90 $3.00 + 0.00

Turbulence structure and heat transfer of a two-dimensional impinging jet with gas–solid suspensions

H. YOSHIDA, K. SUENAGA† and R. ECHIGO
Department of Mechanical Engineering, Tokyo Institute of Technology, Tokyo 152, Japan

(*Received* 17 *May* 1989 *and in final form* 31 *July* 1989)

Abstract—The heat transfer mechanism of a two-dimensional impinging jet with gas–solid suspensions has been investigated through flow measurements using laser-Doppler anemometry. The most striking feature of the flow is the presence of particles rebounding from the impingement plate and of the gas-phase reverse flow caused by those particles. As a result, the turbulent intensity normal to the plate increases markedly near the stagnation point. However, in the wall jet region where the gas–solid interaction is relatively weak, the turbulence structure undergoes only a slight change. Heat transfer experiments in which the loading ratio is varied from 0 to 0.8 have been conducted. Around the stagnation point, the Nusselt number reaches 2.7 times as great as that of the single-phase flow, and the heat transfer enhancement is ascribed to the drastic change in the turbulence structure.

1. INTRODUCTION

IT SOMETIMES happens that a small amount of additives causes an amazing change in a system. Enhancement of heat transfer in gas flows by means of solid additives is a typical example of such situations [1, 2]. Among many heat transfer systems with gas–solid suspensions, the most pronounced enhancement has been observed in heat transfer by impinging jets.

Shimizu *et al.* [3] experimentally investigated the heat transfer of an axisymmetric jet impinging on a flat surface. They used a suspension consisting of nitrogen gas and graphite particles of 10 μm diameter, and varied the initial loading ratio (defined as the ratio of the total solid mass flow rate to the mass flow rate of gas at a nozzle exit) up to 2.5. The stagnation-point heat transfer coefficient obtained at the highest loading ratio was found to be six times as large as that for the single-phase flow. Shimizu *et al.* [4] also carried out an experiment on a two-dimensional jet impinging on a concave surface, and observed that heat transfer in the wall jet region is effectively enhanced in comparison with that for a flat surface.

To evaluate the contribution of various factors to the heat transfer enhancement, Shimizu *et al.* [4] introduced the modified Reynolds and Stanton numbers which take account of the increases in momentum and in heat capacity due to the particle addition. By comparing the modified Reynolds–Stanton correlation with the original correlation for the single-phase flow, they attributed the heat transfer enhancement principally to the production of turbulence in the viscous sublayer by particles. They stated that such a gas–solid interaction results from the large difference between the inertia forces, and that the interaction is further enhanced if the streamlines of the two phases cross each other. Kurosaki *et al.* [5] also conducted heat transfer experiments on an axisymmetric impinging jet with particles of various sizes and materials. They remodified the Stanton number previously modified by Shimizu *et al.* [4] so as to include the effect of the direct contact heat transfer between the heated surface and particles.

In these studies, however, the heat transfer characteristics are examined only in terms of the macroscopic dimensionless parameters. Hence, the main discussions on the heat transfer mechanism are not based on conclusive experimental evidence. To elucidate the mechanism fundamentally, it is necessary to know the structure of turbulence, which is changed by the interaction between gas and solid phases. The laser-Doppler anemometry (LDA) developed for gas–solid two-phase flows [6–12] is a powerful means to this end, and has been applied to measurements for two-phase free and wall jets [10, 13–16]. However, the two-phase impinging jet in which the stronger gas–solid interaction may occur has not yet been investigated.

The objective of the present study is to provide detailed data on the turbulence structure and, on the basis of this information, to clarify the heat transfer mechanism of the gas–solid impinging jet. A two-dimensional system is chosen for convenience of LDA measurements.

2. APPARATUS AND TECHNIQUES

2.1. *Flow configuration*

A schematic diagram of the experimental facility is shown in Fig. 1. After the air was filtered upstream of

† Present address: Mitsubishi Heavy Industries, Ltd., Tokyo 100, Japan.

NOMENCLATURE

B	nozzle width [m]
C	constant for accelerating the free stream around a two-dimensional stagnation point [s^{-1}]
n	particle passing rate [s^{-1}]
Nu	Nusselt number, $\alpha B/\lambda$
Pr	Prandtl number
Re	Reynolds number, $\lvert W_{g0}\rvert B/\nu$, $\lvert W_0\rvert B/\nu$
U_∞	mean velocity outside the boundary layer, Cx [$m\,s^{-1}$]
U, W	mean velocity components in the x- and z-directions [$m\,s^{-1}$]
u, w	fluctuating velocity components in the x- and z-directions [$m\,s^{-1}$]
x, z	coordinates fixed to the impingement plate [m]
z_n	nozzle-to-plate spacing [m].

Greek symbols

α	heat transfer coefficient [$W\,m^{-2}K^{-1}$]
Γ	loading ratio
λ	thermal conductivity of gas [$W\,m^{-1}K^{-1}$]
ν	kinematic viscosity of gas [m^2s^{-1}].

Subscripts

g	gas phase
s	solid phase
0	value at nozzle exit.

Superscripts

+	particle rebounding from plate
−	particle approaching plate
—	time average.

the blower, micrometer-sized talc particles were added to provide seeding for the LDA. Spherical glass beads were introduced into the air flow via a screw feeder. An injection channel 10 mm wide and 1200 mm long was used to provide a fully developed turbulent channel flow at the exit nozzle. At the front and rear ends of the test section, windows for LDA measurements were attached. A cyclone was installed at the end of the flow system to separate the glass particles from the air flow. Since the flow through the cyclone was induced mainly by a suction blower, the flow-rate (pressure) control is difficult if the flow duct is perfectly closed. Hence, two auxiliary inlets for ambient air were provided at the location downstream of the impingement plate.

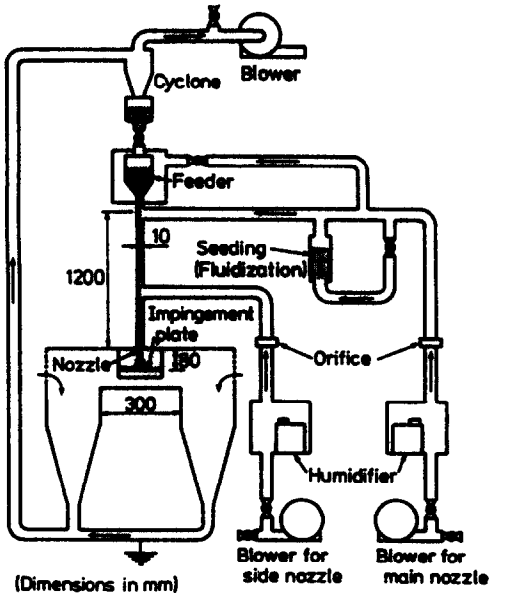

FIG. 1. Schematic of experimental facility.

In the operations of gas–solid two-phase flows, the static electricity charged in fine particles often exerts unexpected effects on the flow and temperature fields. To reduce these effects, humidifiers were installed downstream of the blowers, and the relative humidity was maintained at about 65% throughout the experiments. Furthermore, the duct was made of electrically conductive material and grounded. Consequently, static electricity was almost completely suppressed, and good reproducibility of flow and heat transfer measurements was achieved.

Figure 2 shows the detail of the flow configuration. The main nozzle (aspect ratio, 8) was located between two side nozzles (aspect ratio, 3) through which the flows without solid particles were injected so as to prevent the windows from becoming coated with particles. Two impingement plates were used. One, for LDA measurements, was a transparent glass plate through which one laser beam passed obliquely so as to intersect the other in the vicinity of the plate. The other was a constant-heat-flux heat transfer measurement plate.

As indicated in Fig. 2, the stagnation point is taken as the coordinate-system origin; x and z denote distance parallel to and normal to the surface, respectively. The mean and fluctuating velocity components in each direction are denoted by (U, u) and (W, w). The subscripts g and s denote the gas and the solid phase, respectively, while velocities for single-phase flow are given without any subscripts.

The mean diameter of the glass beads used in the present work was 48.9 μm, and its standard deviation was 8.7 μm. This particle size is much larger than that

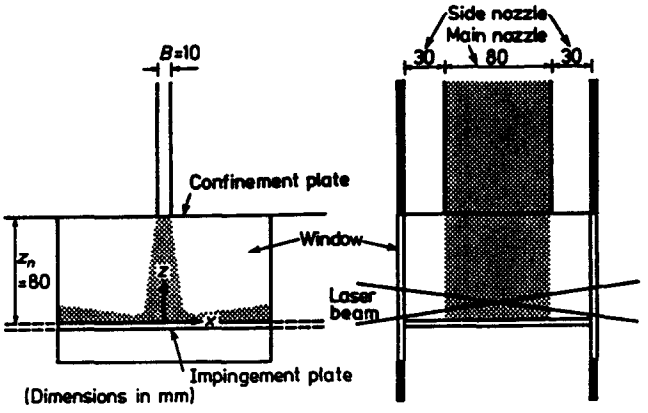

FIG. 2. Detail of flow configuration.

used by Shimizu *et al.* [3, 4]; in the choice of size, the requirements of LDA measurements described below were taken into account.

2.2. *Laser-Doppler anemometry and signal processing*

The laser-Doppler anemometry was operated in the fringe and forward-scattering modes. A block diagram of the optical and signal processing system is shown in Fig. 3. The optical system consisted of a 25 mW He–Ne laser, integrated transmission optics with a Bragg cell, and light-collecting optics with photomultiplier; light frequency shifting was required to measure the reverse flow caused by particles rebounding from the impingement plate. Two components of mean velocity (U, W) and the Reynolds stresses $\overline{u^2}$, $\overline{w^2}$, $\overline{uw}$ were calculated from the data of three velocity components obtained by rotating the integrated transmission optics about their axes at angles of $\pm 45°$ [17].

The solid-phase velocity was easily measured in the absence of seeding particles. However, for the gas-phase velocity measurement in the presence of solid particles, the signals from the solid particles should be rejected. The signal discrimination method employed in the present study (Fig. 3) was basically the same as that developed by Maeda *et al.* [8] and Hishida *et al.* [10]. Hence, an explanation of it has been omitted here. For the data reduction, more than 2000 digital outputs from the LDA counter were processed by an on-line microcomputer system.

2.3. *Heat transfer measurement*

The heat transfer measurement plate consists of a stainless steel foil (30 μm thick) glued to a bakelite backing. For the wall temperature measurement, 13 thermocouples (type T, 0.1 mm diameter) were embedded under the stainless steel foil. Alternating current was supplied to the foil to provide a constant heat flux from the surface. The back surface of the plate was insulated by glass wool, and the resulting conduction through the insulation accounts for less than 3% of the total heat transfer from the foil. The heat transfer coefficient was determined by measuring the difference between the wall and free-stream temperatures.

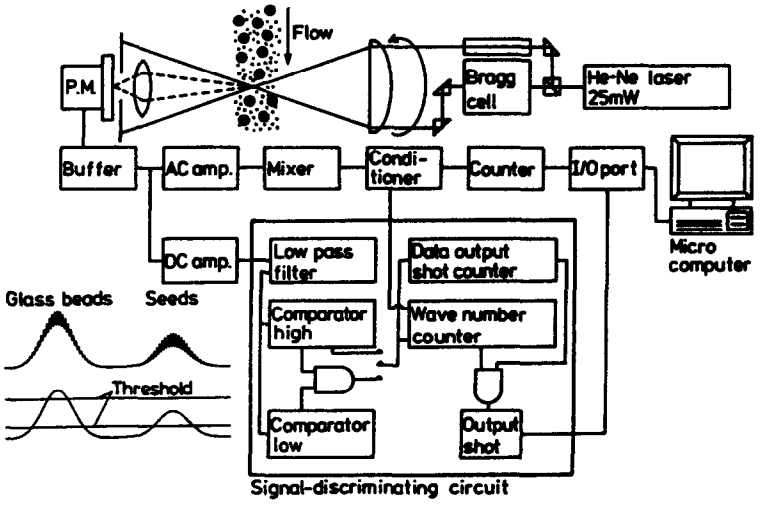

FIG. 3. Block diagram of optical and signal processing system for LDA measurements.

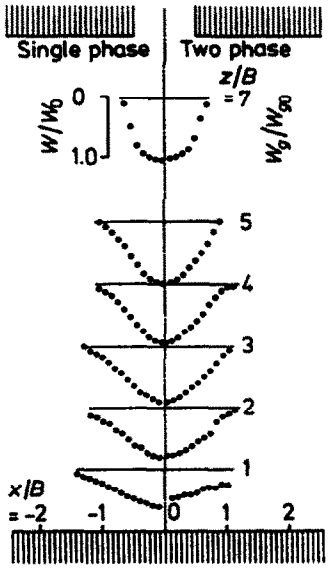

FIG. 4. Profiles of gas-phase mean velocity upstream of stagnation point.

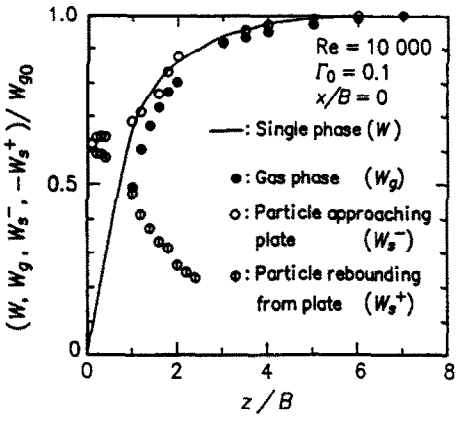

FIG. 5. Variations of axial velocities along stagnation streamline.

3. RESULTS AND DISCUSSION

In the present experiments, the dimensionless nozzle-to-plate spacing was held constant at $z_n/B = 8$. This choice was based on the fact that the heat transfer coefficient of single-phase impinging jets reaches a maximum in the neighborhood of $z_n/B = 8$ [18–20]. The Reynolds number $Re = |W_{g0}|B/\nu$, where W_{g0} is the bulk-mean gas velocity at the nozzle exit, was fixed at 10000. The initial loading ratio Γ_0 was varied up to 0.8 in the heat transfer experiments. However, in the flow measurements using LDA, Γ_0 was fixed at 0.1. This is because Γ_0 was limited to a maximum of 0.1 owing to the flow turbidity. Although this upper limit seems to be lower than expected, highly dense suspensions exist in the vicinity of the stagnation point (where the gas phase is stagnant), even if the initial loading ratio Γ_0 is small.

3.1. *Flow characteristics*

3.1.1. *Upstream region of stagnation point.* The profiles of the gas-phase mean velocity are shown in Fig. 4. The profiles to the left of the centerline are for the single-phase flow; those to the right are for the two-phase flow. At $z/B > 3$, the spreading rate of the two-phase jet is slightly lower than that of the single-phase flow. Since the flow is not so different from usual free jets in this region, the reduction in the spreading rate is attributed to two effects as reported in the previous studies on the free jets [13, 15, 16]: one effect is the momentum transfer from the particles to the gas; the other effect is the modulation of the gas turbulence caused by the particles. At $z/B = 1$, where the impingement plate exerts a considerable influence on the flow, the profiles are appreciably different from each other.

For more detailed examination of the time-mean velocity field, the variations of the axial velocities along the stagnation streamline ($x/B = 0$) are presented in Fig. 5; a solid circle denotes the gas-phase mean velocity (W_g), while open and split circles denote the mean velocities of particles approaching or rebounding from the plate (W_s^- and W_s^+), respectively. At $z/B < 2$, the gas-phase velocity rapidly decreases owing to the presence of the impingement plate, but the solid-phase velocity does not because of the large inertia of particles. As a result, the particles collide with the plate at a high velocity, and rebound from it. (Since both the particles and the impingement plate are made of glass, the collision is practically elastic.) It is interesting that some particles go upstream against the oncoming gas flow and reach about $z/B = 2.5$; such particle behavior was confirmed by simple numerical analysis for a single particle moving along the stagnation streamline.

Figure 6 shows the streamwise variation of the particle passing rate n. Here, the particle passing rate is defined as the time-averaged number of particles passing the LDA measuring volume per unit time. The gradual increase in n/n_0 at $z/B < 3$ also indicates the presence of the rebounding particles.

To clearly show the particle effect on the flow field,

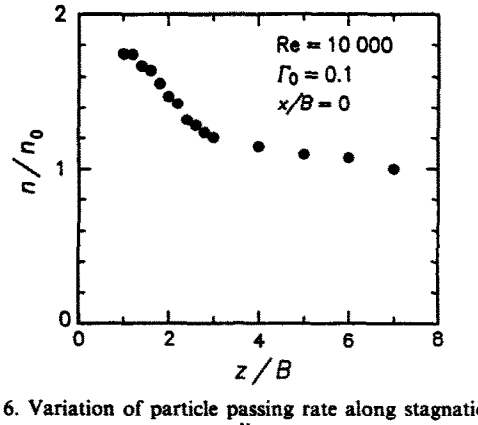

FIG. 6. Variation of particle passing rate along stagnation streamline.

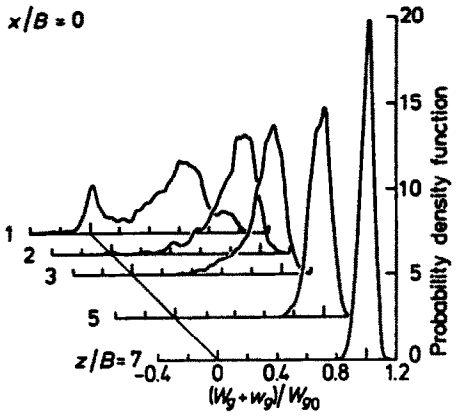

FIG. 7. Probability density functions of gas-phase velocity on stagnation streamline.

we present the probability density functions (PDFs) of the gas-phase velocity for various z/B in Fig. 7. The most striking feature of the figure is that there are two peaks in the PDF at $z/B = 1$. Whereas the peak for higher $(W_g+w_g)/W_{g0}$ corresponds to the flow approaching the plate, that around $(W_g+w_g)/W_{g0} = 0$ demonstrates the reverse flow associated with the rebounding motion of particles.

The profiles of turbulent intensities and Reynolds shear stress are shown in Fig. 8. In the free jet region ($z/B > 3$), the turbulence modulation by the particles discussed in conjunction with Fig. 4 is not so clear; this is because the initial loading ratio in the present experiment is small ($\Gamma_0 = 0.1$). Irrespective of whether the flow is single or two phase, the profiles of the axial components ($\sqrt{(\overline{w^2})}$ and $\sqrt{(\overline{w_g^2})}$) usually have their maxima at the locations where the mean strain rates (accordingly, the Reynolds shear stresses $-\overline{uw}$ and $-\overline{u_g w_g}$) are largest. The single exception, however, is the profile of $\sqrt{(\overline{w_g^2})}$ at $z/B = 1$; it has a maximum at $x/B = 0$, where the number density of solid particles is considered to be largest. Therefore, the interaction between gas and rebounding particles is responsible for the intensification of $\sqrt{(\overline{w_g^2})}$ near the stagnation point. It should be noted here that in the two-phase free flows [13, 15, 16] particles generally cause a reduction in the gas turbulence and an increase in the dissipation rate of that energy. However, in the present impinging jet, the particle velocity relative to the gas is so large (the particle Reynolds number is more than 50) that the turbulence is generated by the wake of the particles. The strength of the interaction depends chiefly on the following three factors: the number density of particles, the slip velocity, and the difference between the flow directions of the two phases. Near the stagnation point, all three factors contribute to enhancement of the interaction.

In contrast to those of the axial component, the profiles of the lateral intensities ($\sqrt{(\overline{u^2})}$ and $\sqrt{(\overline{u_g^2})}$) are qualitatively similar to each other, although $\sqrt{(\overline{u_g^2})}$ is larger than $\sqrt{(\overline{u^2})}$ in the region near the stagnation point. The same is true in Reynolds shear stresses $-\overline{uw}$ and $-\overline{u_g w_g}$, which are generated by $\overline{u^2}\partial W/\partial x$ and $\overline{u_g^2}\partial W_g/\partial x$, respectively (cf. ref. [21]).

Figure 9 displays the variations of turbulent intensities along the stagnation streamline. In the stagnation flow with free-stream turbulence, the axial component of the Reynolds stresses is selectively intensified by the strongly diverging flow near the stagnation point; the resulting anisotropy between the axial and lateral components contributes to the augmentation of the total turbulence energy [22].

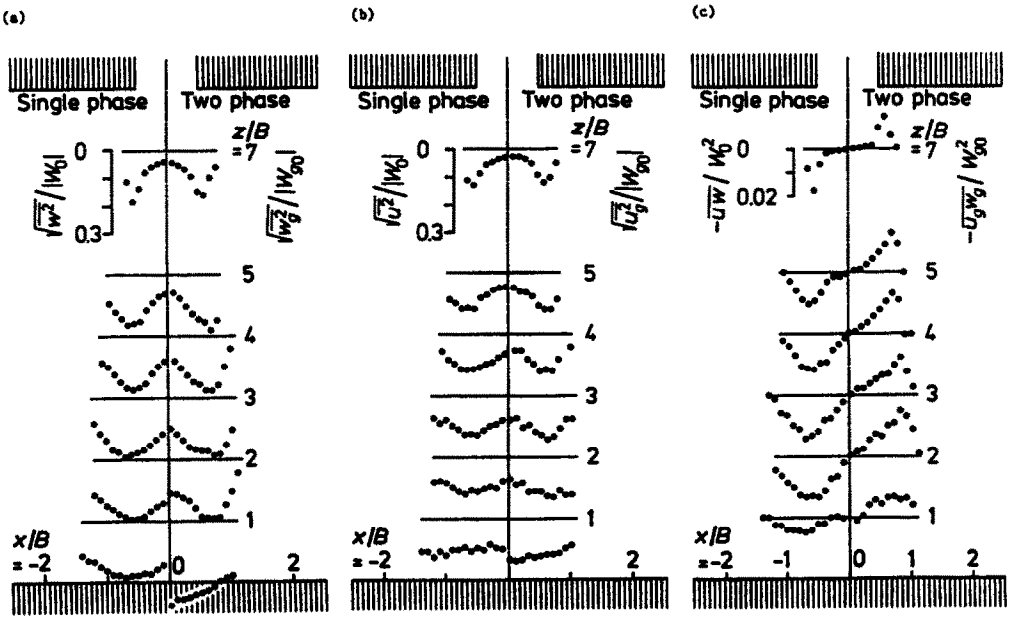

FIG. 8. Profiles of turbulent intensities and Reynolds shear stress upstream of stagnation point: (a) axial intensity; (b) lateral intensity; (c) Reynolds shear stress.

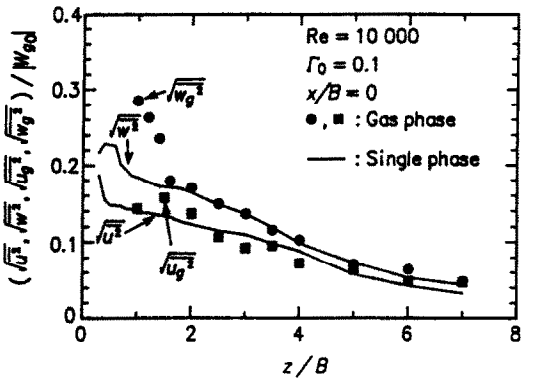

FIG. 9. Variations of turbulent intensities along stagnation streamline.

These features are also seen in the data for the single-phase flow at $z/B < 1$ in Fig. 9. In the two-phase flow, the anisotropy is further amplified by the gas–solid interaction.

3.1.2. *Downstream region of stagnation point.* Figures 10 and 11 show the profiles of lateral mean velocities and turbulent intensities in the downstream region of the stagnation point. (The fluctuating velocity normal to the wall, which is important to discuss the wall heat transfer, could not be measured because of the very poor quality of the laser-Doppler signals.)

At $x/B = 1$, the turbulent intensity for the two-phase flow is maximally about 50% larger than that for the single-phase flow. The cause of the intense turbulence in this region is considered to be the interaction between the gas flowing along the plate and the particles the moving direction of which is mainly normal to the plate. On the other hand, the peak velocity for the gas phase is about 20% smaller than that for the single-phase flow. This is because particles initially having no momentum in the x-direction become a burden to the gas phase.

At $x/B = 4$, the difference between the gas-phase and the single-phase velocities is slight near the wall. In the region far from the wall ($z/B > 0.4$), however, the gas-phase velocity is larger than that of the single-phase flow; this is because the rebounding particles accelerated near the stagnation point pass through this region.

As the distance x from the stagnation point increases, the gas-phase turbulent intensity in the near

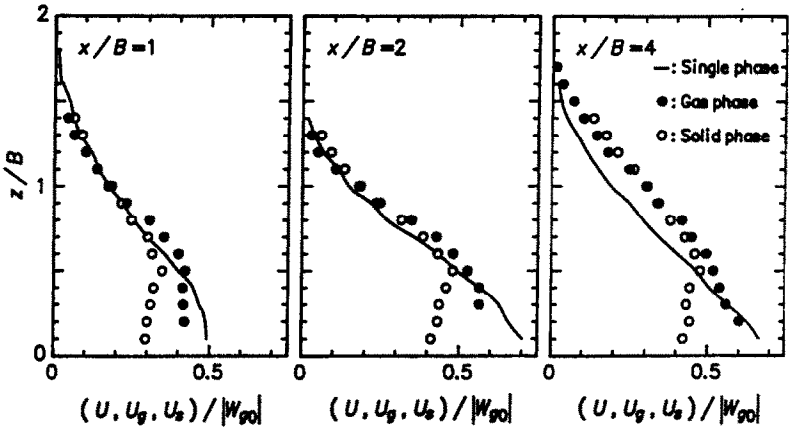

FIG. 10. Profiles of mean velocities downstream of stagnation point.

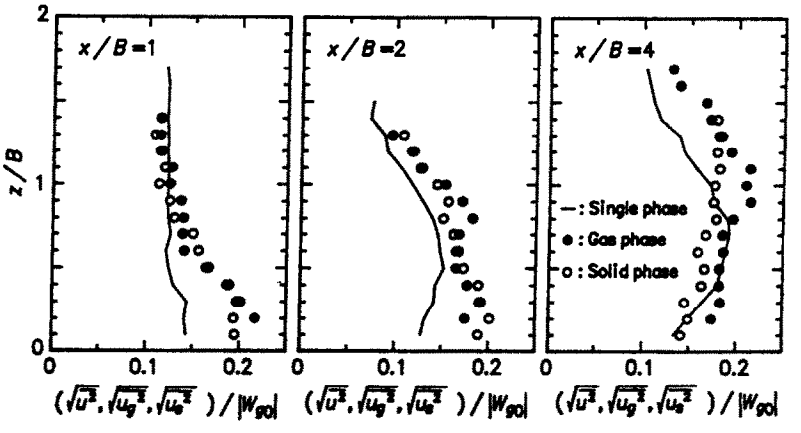

FIG. 11. Profiles of turbulent intensities downstream of stagnation point.

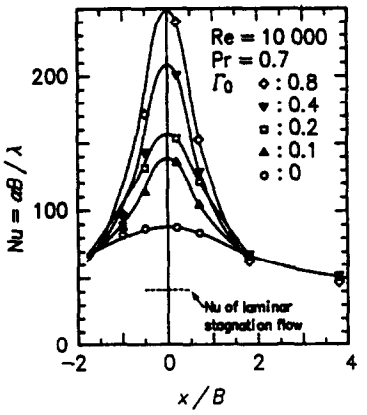

FIG. 12. Distributions of Nusselt number.

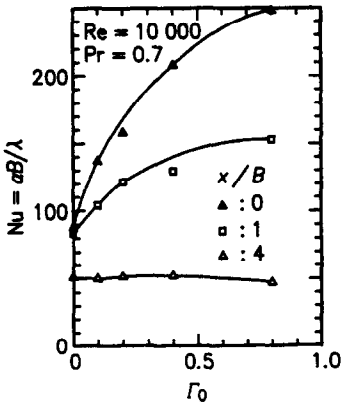

FIG. 13. Effect of loading ratio on Nusselt number.

wall region decreases and approaches the level for the single-phase flow (Fig. 11). This trend is attributed to the attenuation of the gas–solid interaction with increasing distance x.

Further downstream (beyond the range of x/B in this experiment), the turbulence intensity may fall below that in the single-phase flow, as reported in the study on a two-phase wall jet [14].

3.2. *Heat transfer characteristics*

The results of the heat transfer measurements for various loading ratios Γ_0 are presented in Fig. 12. The broken line in the figure shows the Nusselt number of the laminar stagnation flow calculated using the measured static pressure distribution for $\Gamma_0 = 0$. That is, the heat transfer coefficient of the laminar stagnation flow is theoretically given by

$$\alpha = 0.57\lambda(C/\nu)^{0.5} Pr^{0.4} \quad (1)$$

where C is a constant for the accelerating free stream outside the boundary layer ($U_\infty = Cx$) [23]. The measured Nusselt number for $\Gamma_0 = 0$ results in an approximately twofold increase. This trend was also observed in the previous study on a two-dimensional impinging jet [20].

All the Nusselt number profiles show the same general features: with increasing loading ratio, the Nusselt number markedly increases in the vicinity of the stagnation point ($x/B < 1.5$). The maximum Nusselt number obtained in the present experiment is 2.7 times as great as that of the single-phase flow. On the other hand, at $x/B > 1.5$, there is virtually no change.

Here, it should be noted that the heat transfer characteristics of the present flow strongly depend on humidity (or static electricity charged in particles). For example, a preliminary experiment at relative humidity of 40% showed that the heat transfer characteristics hardly change, irrespective of the variation of the loading ratio, and in this case the reproducibility of flow and heat transfer measurements was poor. However, for the experiments in which relative humidity was larger than 65%, the reproducibility was satisfactory. Thus, the following discussion is valid for the case of such somewhat high relative humidity.

3.3. *Heat transfer mechanism*

The velocity and thermal boundary layers developed over the impingement plate are so thin (their minimum thickness is less than 1 mm) that data on the flow field inside the boundary layers could not be obtained in the present experiments. However, the study on the heat transfer in the single-phase stagnation flow demonstrated that the turbulence in the oncoming flow exerts a decisive influence on heat transfer characteristics [22]. Furthermore, according to the estimation of Kurosaki *et al.* [5], the efficiency of the direct contact heat transfer for glass beads of 50 μm diameter is of the order of 0.1%. Therefore, it is reasonable to discuss the present heat transfer results in the light of the turbulence structure in the oncoming flow.

On the basis of a comparison of Fig. 12 with Figs. 8 and 9, we can attribute the heat transfer enhancement around the stagnation point to the marked increase in the axial (normal) component of turbulent intensity. The decreasing heat-transfer enhancement with increasing distance x corresponds to the reduction of the turbulence energy generated by the gas–solid interaction (Fig. 11). The heat transfer mechanism at much larger x/B, i.e. in the developed wall jet region, is discussed by Hishida *et al.* [14].

In Fig. 13, the Nusselt numbers at $x/B = 0$, 1 and 4 are plotted against the loading ratio Γ_0. As clearly seen from the figure, the dependency of Nu on Γ_0 is nonlinear. This fact also indicates that the direct contact heat transfer between particles and the plate is not a dominant mode of heat transfer enhancement. (Provided that the direct contact heat transfer is dominant, the increase in Nu should be proportional to Γ_0.)

4. CONCLUSIONS

The detailed turbulence structure of the two-dimensional impinging jet with gas–solid suspensions was

measured by means of laser-Doppler anemometry. The large difference between the inertia forces of gas and solid phases is responsible for all of the gas–solid interactions. The most notable feature of the flow is the presence of particles rebounding from the impingement plate and going upstream against the oncoming flow. This feature sharply distinguishes the gas–solid impinging jet from other gas–solid flows, such as free and wall jets. The resulting gas–solid interaction near the stagnation point is violent and induces gas-phase reverse flow. The combined heat-transfer and fluid-dynamic measurements indicate that the mechanism of the heat transfer enhancement around the stagnation point is attributable to the drastic change in the turbulence structure.

REFERENCES

1. A. E. Bergles, Techniques to augment heat transfer. In *Handbook of Heat Transfer Applications* (Edited by W. M. Rohsenow, J. P. Hartnett and E. N. Ganic), 2nd Edn, pp. 3-1–3-80. McGraw-Hill, New York (1985).
2. S. Hasegawa, R. Echigo and A. Shimizu, Convective and radiative heat transfer of flowing gaseous–solid suspensions. In *Handbook of Heat and Mass Transfer* (Edited by N. P. Cheremisinoff), Vol. 1, pp. 523–557. Gulf, Houston, Texas (1986).
3. A. Shimizu, R. Echigo and S. Hasegawa, Impinging jet heat transfer with gas–solid suspension medium, *Advances in Enhanced Heat Transfer, Proc. 18th National Heat Transfer Conf.*, San Diego, California, pp. 155–160 (1979).
4. A. Shimizu, K. Fukamichi and S. Hasegawa, Impinging jet heat transfer of gaseous suspension on concaved surface, *Trans. JSME*, Ser. B (in Japanese) **51**, 1349–1354 (1985).
5. Y. Kurosaki, T. Murasaki, I. Satoh and T. Kashiwagi, Study on heat transfer mechanism of a gas–solid suspension impinging jet (effect of particle sizes and thermal properties). In *Heat Transfer 1986* (Edited by C. L. Tien, V. P. Carey and J. K. Ferrell), Vol. 5, pp. 2587–2592. Hemisphere, Washington, DC (1986).
6. F. Durst, Studies of particle motion by laser Doppler techniques, *Proc. Dynamic Flow Conf.*, Marseille, pp. 345–372 (1978).
7. S. L. Lee and J. Srinivasan, Measurement of local size and velocity probability density distributions in two-phase suspension flows by laser-Doppler technique, *Int. J. Multiphase Flow* **4**, 141–155 (1978).
8. M. Maeda, K. Hishida and T. Furutani, Optical measurements of local gas and particle velocity in an upward flowing dilute gas–solids suspension, *ASME Proc. Polyphase Flow and Transport Technology*, San Francisco, California, pp. 211–216 (1980).
9. K. Hishida, M. Maeda, J. Imaru, K. Hironaga and H. Kano, Measurements of size and velocity of particle in two-phase flow by a three beam LDA system, *Proc. 1st Int. Symp. on Applications of Laser Anemometry to Fluid Mechanics*, Lisbon, 5.6 (1982).
10. K. Hishida, K. Tajima, M. Maeda and H. Kano, Measurements of two-phase turbulent flow by LDA with particle size discrimination, *Proc. 2nd Int. Symp. on Applications of Laser Anemometry to Fluid Mechanics*, Lisbon, 18.4 (1984).
11. Y. Tsuji and Y. Morikawa, LDV measurements of an air–solid two-phase flow in a horizontal pipe, *J. Fluid Mech.* **120**, 385–409 (1982).
12. D. Modarress and H. Tan, LDA signal discrimination in two-phase flows, *Exp. Fluids* **1**, 129–134 (1983).
13. K. Hishida, K. Kaneko and M. Maeda, Turbulence structure of gas–solids two-phase circular jet, *Trans. JSME*, Ser. B (in Japanese) **51**, 2330–2337 (1985).
14. K. Hishida, K. Umemura and M. Maeda, Heat transfer to plane wall jet in gas–solids two-phase flow. In *Heat Transfer 1986* (Edited by C. L. Tien, V. P. Carey and J. K. Ferrell), Vol. 5, pp. 2385–2390. Hemisphere, Washington, DC (1986).
15. D. Modarress, H. Tan and S. Elghobashi, Two-component LDA measurement in a two-phase turbulent jet, *AIAA J.* **22**, 624–630 (1984).
16. A. A. Mostafa, H. C. Mongia, V. G. McDonell and G. S. Samuelsen, Evolution of particle-laden jet flows: a theoretical and experimental study, *AIAA J.* **27**, 167–183 (1989).
17. S. E. Logan, A laser velocimeter for Reynolds stress and other turbulence measurements, *AIAA J.* **10**, 933–935 (1972).
18. R. Gardon and J. C. Akfirat, The role of turbulence in determining the heat-transfer characteristics of impinging jets, *Int. J. Heat Mass Transfer* **8**, 1261–1272 (1965).
19. R. Gardon and J. C. Akfirat, Heat transfer characteristics of impinging two-dimensional air jets, *ASME J. Heat Transfer* **88**, 101–108 (1966).
20. M. Kumada and I. Mabuchi, Studies on heat transfer by impinging jet (1st report, Flow and mass transfer by two-dimensional air jet directed normal to a flat plate), *Trans. JSME* (in Japanese) **35**, 1053–1061 (1969).
21. W. Rodi, A review of experimental data of uniform density free turbulent boundary layers. In *Studies in Convection* (Edited by B. E. Launder), Vol. 1, pp. 79–165. Academic Press, London (1975).
22. K. Hijikata, H. Yoshida and Y. Mori, Theoretical and experimental study of turbulence effects on heat transfer around the stagnation point of a cylinder. In *Heat Transfer 1982* (Edited by U. Grigull, E. Hahne, K. Stephan and J. Straub), Vol. 3, pp. 165–170. Hemisphere, Washington, DC (1982).
23. W. M. Kays and M. E. Crawford, *Convective Heat and Mass Transfer*, 2nd Edn, pp. 139–141. McGraw-Hill, New York (1980).

STRUCTURE DE LA TURBULENCE ET TRANSFERT THERMIQUE D'UN JET BIDIMENSIONNEL IMPACTANT AVEC SUSPENSION GAZ–SOLIDE

Résumé—Le mécanisme de transfert thermique d'un jet bidimensionnel impactant avec suspension gaz–solide est étudié par anémométrie laser-Doppler. Le fait marquant de l'écoulement est la présence des particules qui rebondissent sur la plaque et celle d'un écoulement de retour de la phase gazeuse causé par ces particules. Il en résulte que l'intensité de turbulence normale à la plaque croît fortement près du point d'arrêt. Néanmoins dans la région du jet pariétal où l'interaction gaz–solide est relativement faible, la structure de turbulence est faiblement modifiée. Des expériences de transfert thermique, dans lesquelles le rapport de charge varie de zéro à 0,8 ont été faites. Autour du point d'arrêt, le nombre de Nusselt atteint une valeur 2,7 fois plus grande que dans le cas d'une simple phase et l'accroissement de transfert est lié au grand changement de la structure de la turbulence.

TURBULENZSTRUKTUR UND WÄRMEÜBERGANG IN EINEM ZWEIDIMENSIONALEN AUFTREFFENDEN STRAHL EINER GAS-FESTSTOFF-SUSPENSION

Zusammenfassung—Es wird der Mechanismus der Wärmeübertragung in einem zweidimensionalen auftreffenden Strahl aus Gas-Feststoff-Suspensionen untersucht. Die Strömungsmessungen werden mit einem Laser-Doppler-Anemometer durchgeführt. Das auffallendste Merkmal der Strömung ist die Anwesenheit von Teilchen, die von der Auftreffplatte zurückprallen, und einer Gasrückströmung, die durch Teilchen verursacht wird. Daraus resultiert eine merkliche Zunahme der Turbulenzintensität senkrecht zur Platte in der Nähe des Stagnationspunktes. Im Wandbereich jedoch, wo die Wechselwirkung zwischen Gas und Feststoff relativ schwach ist, erfährt die Turbulenzstruktur eine leichte Änderung. Es wurden Experimente zum Wärmeübergang bei einem Beladungsverhältnis von 0 bis 0,8 durchgeführt. In der Umgebung des Stagnationspunkts ist die Nusselt-Zahl 2,7 mal größer als bei einphasiger Strömung. Die Verbesserung des Wärmeübergangs wird der drastischen Änderung der Turbulenzstruktur zugeschrieben.

СТРУКТУРА ТУРБУЛЕНТНОСТИ И ТЕПЛОПЕРЕНОС В ЛВУМЕРНОЙ СТРУЕ ГАЗА С ТВЕРДЫМИ ЧАСТИЦАМИ, НАБЕГАЮЩЕЙ НА ПЛАСТИНУ

Аннотация—При помощи измерений потока с применением лазер-доплеровской анемометрии исследуется механизм теплопереноса в случае двумерной набегающей на пластину струи газа с твердыми частицами. Наиболее характерной особенностью течения является наличие частиц, отскакивающих от пластины, и вызванного ими противотока газовой фазы. В результате перпендикулярная к пластине составляющая интенсивности турбулентности ощутимо возрастает вблизи точки торможения. Однако в пристенной области струи, где взаимодействие газа и твердых частиц является сравнительно слабым, структура турбулентности претерпевает лишь незначительное изменение. Проведены эксперименты по теплопереносу с варьированием отношения нагрузок эт 0 до 0,8. Вокруг точки торможения значение числа Нуссельта в 2,7 раз больше, чем при однофазном течении, и интенсификация теплопереноса объясняется сильным изменением структуры турбулентности.